metals

MDPI

Article

Effect of Deformation on Precipitation and the Microstructure Evolution during Multistep Thermomechanical Processing of Al-Zn-Mg-Cu Alloy

Jinrong Zuo [1,2,*], Longgang Hou [3], Xuedao Shu [1,2], Wenfei Peng [1,2], Anmin Yin [1,2] and Jishan Zhang [3]

1 College of Mechanical Engineering and Mechanics, Ningbo University, Ningbo 315211, China; shuxuedao@nbu.edu.cn (X.S.); pengwenfei@nbu.edu.cn (W.P.); yinanmin@nbu.edu.cn (A.Y.)
2 Zhejiang Provincial Key Laboratory of Part Rolling Technology, Ningbo 315211, China
3 State Key Laboratory for Advanced Metals and Materials, University of Science and Technology Beijing, 30 Xueyuan Road, Haidian District, Beijing 100083, China; lghou@skl.ustb.edu.cn (L.H.); zhangjs@skl.ustb.edu.cn (J.Z.)
* Correspondence: zuojinrong@nbu.edu.cn; Tel.: +86-0571-87600534

Received: 24 September 2020; Accepted: 21 October 2020; Published: 23 October 2020

Abstract: In order to obtain fine grained structure efficiently, a new multi-step rolling process (MSR: pre-deformation + intermediate annealing + hot deformation) was applied in Al-Zn-Mg-Cu plates. Conventional hot rolling (CHR) was also carried out as a contrast experiment. The evolution of microstructures and improvement of mechanical properties were analyzed by optical microscope, scanning electron microscope, transmission electron microscope, X-ray diffractometer, and tensile tests. The results show that the MSR process can obtain finer longitudinal grain size and better mechanical properties than CHR, which can be explained as follows: spheroidization of precipitates wrapped by high density dislocations could be promoted by increased pre-deformation; numerous ordered substructures were formed during short-period intermediate annealing at high temperature; in the subsequent hot rolling process, the retained spherical precipitates pinned dislocations and boundaries. With the increase of accumulated strain, low angle grain boundaries gradually transformed into high angle grain boundaries, leading to grain refinement. With the increased pre-deformation (MSR_1 20 + 60%, MSR_2 40 + 40%, MSR_3 60 + 20%), the effect of grain refinement and plasticity improvement gradually weakened. The optimum thermomechanical process (MSR_1 solid solution + pre-deformation (300 °C/20%) + intermediate annealing (430 °C/5 min) + hot deformation (400 °C/60%)) was obtained, which can increase elongation by ~25% compared with the CHR process, while maintaining similar high strength for reduced longitudinal grain size.

Keywords: Al-Zn-Mg-Cu alloy; precipitates; hot rolling; microstructure; mechanical property

1. Introduction

Aluminum has been widely used in aerospace, construction, machinery manufacturing, chemical industry, electrical appliances, and other industries [1]. With the development of the industry, the requirements for strength, toughness, and light weight in aerospace are advancing to ever higher levels [2]. Therefore, Al-Zn-Mg-Cu alloys with excellent comprehensive properties, such as high strength-to-weight ratio, good toughness, and stress corrosion cracking resistance, has become one of the most important structural materials applied in aerospace, transportation, and other fields [3]. The main alloying elements of 7xxx series high strength aluminum alloy are Zn, Mg, Cu, Zr, and impurity elements Fe and Si (Zn 7–12%, Mg *wt*% 2–3%). The main strengthening phase is $MgZn_2$. Increasing the content of Zn and Mg can improve the strength, but decreases the toughness and SCC

(stress corrosion resistance). 7xxx series aluminum alloy was developed on the basis of Al-Zn-Mg alloy. Due to serious stress corrosion, the Al-Zn-Mg alloy was limited in wide use until the addition of Cu, Mn, and Cr. In the 1990s, the Alcoa company further increased Zn content on the basis of 7150 alloy composition, to develop the 7055 aluminum alloy under the requirements of maintaining durability and damage tolerance, while improving the strength. Precipitation strengthening is the most effective method for Al-Zn-Mg-Cu alloy. It refers to the strengthening effect caused by the precipitation of the second phase particles, also known as age strengthening. Its physical essence can be explained by the interaction theory between dislocations and second phase particles (the second phase particles and their stress field interact with dislocations and hinder the movement of dislocations). However, the existing Al-Zn-Mg-Cu alloys still have some shortcomings, such as coarse grains, uneven microstructures, and poor plasticity [2], which may limit their wide application and development.

Strength is one of the most important basic mechanical properties of alloys, and can be significantly improved by adding elements to obtain more strengthening phases [4]. However, plasticity and hot workability of the alloy will be greatly deteriorated [5–7]. Fortunately, the decrease of plasticity can be compensated by grain refinement [8,9]. Grains can be micronized or even nano-sized by ECAP (equal channel angular pressing) [10], MDF (multi-directional forging), [11] and CR (cryogenic rolling) [12], but these methods are hard to apply in mass production of large-scale plates, due to the complex process (severe plastic deformation of ECAP or MDF), and high environmental requirements (ultra-low deformation temperature of CR). Thermomechanical processing (TMP) is a strengthening and toughening method, combining deformation and phase transformation to improve the comprehensive properties of aluminum alloy [13]. TMP can increase defect density and modify their arrangement, which affects the nucleation kinetics and distribution of precipitates. Meanwhile, these newly formed precipitates pin and retard the movement of dislocations, stabilize these defects, and refine microstructures, thus improving strength and toughness of the alloy [14]. Yan et al. [15] investigated the effect of deformation temperature on the microstructure and mechanical properties of 7055 aluminum alloy under total strain of 1.6, and found that the sample exhibited a highest ultimate tensile strength of 608 MPa and elongation of 12.5%, with 45% recrystallization grains at the deformation temperature of 400 °C.

Russo et al. [16] had developed a new TMP for 7075 Al alloy (homogenized + deformed at 330 °C and quenched rapidly + recrystallization) to eliminate casting defects and obtain fine grains. The related mechanism was that part of the second phase (chromium rich particles) was dissolved into the matrix during homogenization treatment, and the residue coarse pinned dislocations, to form dislocation stacking during deformation. Therefore, deformation around the coarse second phase particles was more severe, and recrystallization was easier around these coarse second phase particles during subsequent recrystallization treatment. In addition, some stable fine particles were retained after homogenization and distributed at dislocation, sub-grain boundaries and recrystallization grain boundaries, which hindered the boundaries migration. Finally, grains were refined [16]. During TMPs, strain and precipitation, and their interaction, play very important roles. However, these precipitates are not directly involved in the final age strengthening, for all experimental and control samples undergo solutionizing and aging heat treatment after the rolling procedures, destroying any potential differences in strengthening precipitate distribution. The precipitates only play an auxiliary role in grain refinement. Such a process is also called intermediate thermomechanical treatment (ITMP). Waldman et al. [17], improved the process of Russo, E.D. After homogenization, the ingot was furnace cooled, hot rolled, and recrystallized, a similar fine recrystallization structure could be obtained. Wert et al. [18], developed another ITMP process on the basis of the former two. After solution treatment and water quenching, plates were aged for a long time at high temperature. When the size of precipitates reached 0.75–1 μm, water cooling was carried out. Plates were then warm rolled with 90% height reduction, and finally the deformed plates were rapidly heated to the solution temperature. Static recrystallization occurred, and grains were refined. Superplastic plate was successfully manufactured in this way. Esmaeili et al. [19] refined grains of 6xxx series Al alloy by solution natural aging, cold

rolling (80% deformation), and non-isothermal recrystallization annealing (heat rate 0.4 °C/min, starting temperature 50 °C, and ending temperature 380 °C). Grain size of the final plate was about 11 μm on the rolling surface, and 8 μm in the cross section. with uniform distribution. Grain refinement can be achieved by the above-mentioned ITMPs, and the anisotropy can be reduced while maintaining high strength.

However, some shortcomings still exist in existing ITMPs: It takes a long time overaging at high temperature to obtain enough large particles, which is time and energy consuming; It is difficult to deform more than 80% at low temperature (220–300 °C), especially in the center of ultra-high strength Al-Zn-Mg-Cu alloys; The coarse particles obtained by overaging are difficult to re-dissolve completely in a short time during the later solid solution. Additionally, the existing ITMPs are still complex and difficult to apply to large-scale production, so it is necessary to optimize the ITMPs. Therefore, this paper studied the interaction between deformation and precipitation, and developed a new ITMP (MSR: Pre-deformation + SIA (short period intermediate annealing) + final hot rolling) to obtain grain refinement. The MSR process, pre-deformation, intermediate annealing, and final hot deformation are combined to realize the coordinated control of grain refinement and precipitation behavior, and finally achieve good strength and plasticity. Pre-deformation was used to replace the long-term high-temperature overaging of traditional ITMPs, which is time and energy saving. The main deformation stage was set at a high temperature (400 °C) instead of the low-temperature deformation (220–300 °C) of traditional TMPs, leading to small deformation resistance and good formability. The size of the deformation induced precipitates was less than 200 nm, which were be easier to re-dissolve in the final short-term solution, leading to better mechanical properties. Plasticity of the plate was significantly improved, without sacrificing strength. The effect of pre-deformation (MSR_1: 20%, MSR_2: 40%, MSR_3: 60%) on the morphology, area fraction of precipitates, the evolution of microstructure, and the properties of the whole process were studied. A grain refinement model of MSR was built as well.

2. Materials and Methods

Hot rolled commercial 7055 Al alloy plates (Length 75 mm, width 30 mm, thickness 15 mm cut in the middle of 80 mm thick plate, and keeping the rolling direction consistent) with the chemical composition given in Table 1 (Zn, Mg, Cu, Fe, Zr, Ti by IC-AES (electron-coupled plasma atomic emission spectrum), Si by spectrophotometry) were used in this experiment.

Table 1. Chemical composition of AA 7055 alloy (*wt*%).

Element	Zn	Mg	Cu	Zr	Ti	Fe	Si	Al
wt%	8.38	2.07	2.31	0.13	0.16	0.092	0.056	Bal

According to the temperature-precipitates diagram of Al-Zn-Mg-Cu alloy [19], and the correlation constants of the main precipitates [20,21], it can be seen that the volume fraction of M phase (i.e., $MgZn_2$) gradually decreases, while that of S-Al_2CuMg phase increases gradually in the range of 210–435 °C; the volume fraction of S phase decreases gradually in the range of 435–470 °C. That means Al-Zn-Mg-Cu alloy can be regarded as a single-phase solid solution in the temperature range of 470–490 °C; however, when temperature is higher than 490 °C, liquid phase appears, i.e., overburning occurs. Therefore, the optimal solution temperature should be between 470 °C and 490 °C (the interval of single-phase solid solution). The optimum double step (470 °C/16 h + 475 °C/8 h) initialized solution treatment was adopted. After long-term solution treatment, plates were water quenched at room temperature (quenching transfer time less than 10 s). Then, the plates were processed by two routes, shown in Figure 1, with the specific process parameters in Table 2. Route A MSR (Figure 1a): After 20→60% (15→12–6 mm) rolling pre-deformation at 300 °C (according to the Al-$MgZn_2$ pseudo-binary system in our former work [22], the optimum pre-deformation temperature could be set at 300 °C, at which

there was, not only rapid precipitation rate and small deformation resistance, but also a good pinning effect could be obtained), plates were heated to 430 °C (It has been proved that 430 °C cis the optimum temperature for dislocation migration and dislocations rearrangement in our former work [23,24]) for 5 min annealing, and then rolled at 400 °C (consistent with that of the CHR process for comparison) for 60→20% (12~6→3 mm) final deformation. After 7 passes, the total deformation was 80%, with the final plate thickness about 3 mm (15→3 mm). Route B CHR (Figure 1b): SQ-7055 Al plates were rolled for 7 passes at 400 °C for 80% rolling deformation (15→3 mm), and were reheated for 10 min every two passes to retain hot rolling temperature. The hot deformation temperature of route A CHR was set at 400 °C to obtain good microstructure and mechanical properties, according to Yan et al. [15]. All rolled plates (both CHR and MSR) were solution treated at 475 °C for 0.5 h (water quenched at room temperature) and aged at 120 °C for 24 h (T6). The microstructures of samples (e.g., (sub) grain, orientation, second phase, dislocations) were observed by optical microscopy (OM, Zeiss mc80dx, Carl Zeiss AG, Jena, Germany), transmission electron microscopy (TEM, Hitachi H800 and tecnaig2 F30, Hitachi, Tokyo, Japan), scanning electron microscopy (SEM, Zeiss ultra 55, Carl Zeiss AG, Jena, Germany), and X-ray diffraction (XRD, Philips apd210, Philips, Amsterdam, The Netherlands). Size and area fraction of precipitates were counted by the software "Image J". SEM only measures the micron-scale particles. Therefore, the statistics of precipitates were obtained by several TEM images. When the size of precipitates grew to micron-scale, they could be identified by SEM. the changing trends were also verified by SEM images. In order to reduce the effect of error, 3 random TEM images were taken as the average value. Tensile testing was carried out by mechanical testing and simulation (MTS-810, MTS Systems Corporation, Eden Prairie, MN, USA) was used to test mechanical properties at room temperature. The metallographic samples were etched with Keller's reagent (2.5% HNO_3 + 1.5% HCl + 1% HF + 95% H_2O, *vol*%) (Adamas, Shanghai, China). EBSD samples were mechanically and electropolished. The electrolyte was a mixture of 5% $HClO_4$ (Adamas, Shanghai, China) and 95% C_2H_5OH (Adamas, Shanghai, China), the voltage was 30 V, and temperature was from −20 to −30 °C. The Software "Channel 5" (1st, Oxford Instruments, Oxford, U.K.) was used to analyze the EBSD results. Grain boundaries with misorientation <2° could be ignored, with orientations of $2° < \theta < 15°$ defined as LAGBs (LAGBs: Low angle grain boundaries, represented by gray lines), with orientations of $\theta > 15°$ as HAGBs (HAGBs: high angle grain boundaries, represented by black lines). TEM samples were prepared by mechanical grinding the 3 mm diameter sheet to 100 μm, and then thinning by twin-jet electropolishing. The electrolyte was 20% HNO_3 and 80% CH_3OH (*vol*%) (Adamas, Shanghai, China), current was 80–100 mA, and temperature was from −20 to −30 °C. All OM, SEM, EBSD, and TEM were sampled from RD-ND (rolling direction was the normal direction of the cross section) at the mid-thickness layer of the plates.

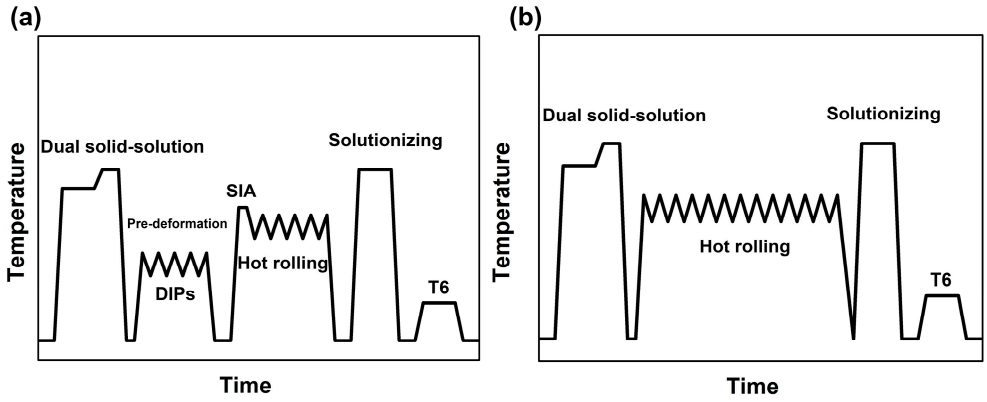

Figure 1. Schematic presentation of thermomechanical processings (TMPs): (**a**) MSR; (**b**) CHR.

Table 2. Specific process parameters.

Process	Pre-Deformation	SIA	Final Hot Rolling
CHR	-	-	400 °C/80%
MSR_1 20 + 60%	300 °C/20% 15→12 mm	430 °C/5 min	400 °C/60% 12→3 mm
MSR_2 40 + 40%	300 °C/40% 15→9 mm		400 °C/40% 9→3 mm
MSR_3 60 + 20%	300 °C/60% 15→6 mm		400 °C/20% 6→3 mm

Note: Pre-deformation—1st step warm rolling, SIA—short time intermediate annealing, final hot rolling—2nd step hot rolling, CHR—conventional hot rolling, MSR—multistep step hot rolling.

3. Results and Discussion

3.1. Microstructure of the Initial Solutionized 7055 Al Alloy

In order to make research meaningful, the initial alloy should return to the homogenization state before hot deformation, that is, the solid solution alloy with uniform microstructure and no segregation. Simultaneously, it is also necessary to ensure that the alloy does not overburn.

The microstructure of the alloy, after initial solution treatment, is shown in Figure 2. It is obvious that static recrystallization occurred during solution treatment. Therefore, some equiaxed grains appeared (Figure 2). However, because of the lack of driving force, the recrystallization was incomplete, so strip-shaped grains were still dominant, with longitudinal ≥600 μm, and transverse ≥200 μm. There was no obvious overburning in the alloy [25], precipitates were dissolved back with more clear grains, shown in Figure 2a. Still some insoluble coarse second phase particles remained at the grain boundaries.

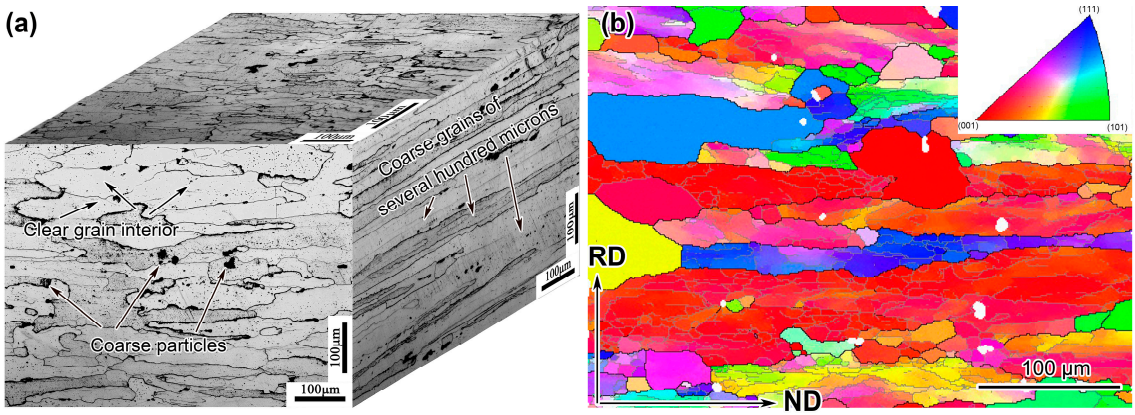

Figure 2. 3D-OM (**a**) and EBSD (**b**) of SQ-7055.

The distribution of high angle grain boundaries (HAGBs) and low angle grain boundaries (LAGBs) of SQ-7055 is shown in Figure 2b. Obvious recrystallization occurred in the alloy, no LAGBs with gray thin lines appeared in the recrystallized grains interior. Grain orientation was still dominated by {001}, and the recrystallization volume fraction was 28.6%. High-density LAGBs appear inside the elongated grains.

3.2. Evolution of Microstructures during TMPs

The purpose of 20→60% pre-deformation of MSR at 300 °C is to obtain sufficient DIPs (Deformation Induced Precipitates) and dislocation accumulation required by the subsequent TMPs. The solid solution state of supersaturated aluminum alloys (such as 7055 Al alloy) is unstable. The decomposition of supersaturated solid solution, and desolvation of solute atoms, can be caused by aging treatment or

deformation under solution temperature, thus affecting the morphology, distribution, and density of precipitates [26].

Figure 3 is SEM images of 7055 Al alloy during TMPs (with embedded TEM images, the white spots in TEM are the precipitates corroded by twin-jet electropolishing). It can be seen from Figure 3(a1) that rod/spherical precipitates along a certain direction were formed after 300 °C/20% warm rolling (pre-deformation) of SQ-7055 Al alloy. With the increased pre-deformation, the size of precipitates increased, while their density decreased (Figure 3(a1–a3)). Spherical precipitates increased while the rod-shaped decreased, as shown in Figure 3(a2,a3). In precipitation strengthening Al alloy, the precipitation and growth of particles is a composite process of thermodynamics and kinetics. With the increased deformation, more defects (such as vacancies, dislocations, deformation bands, etc.) were introduced. These defects, with large structural fluctuation, would become the rapid diffusion channels of solute atoms, which accelerated the atomic diffusion and promoted the growth of precipitates. Therefore, the size of precipitates increased with deformation. The size and area fraction of precipitates, obtained after different pre-deformations, were statistically analyzed. It was found that with increased pre-deformation from 20% to 40%, and 60%, size of precipitates increased from 33 nm to 46 nm, and 58 nm, while their density decreased, but the area fraction maintained similar (5.8%, 5.6%, and 5.9%, respectively, with pre-deformation). As mentioned above, the fast diffusion channels of solute atoms can be formed through numerous defects introduced by strain, which affects the precipitation and re-desolution rate of the second phase particles. However, from the thermodynamic point of view, the solubility of solid solution is affected by temperature. Therefore, the total amount of precipitates (i.e., the area fraction), should also be determined by temperature under the condition of equilibrium state [27]. Strain can only affect the morphology and size of precipitates.

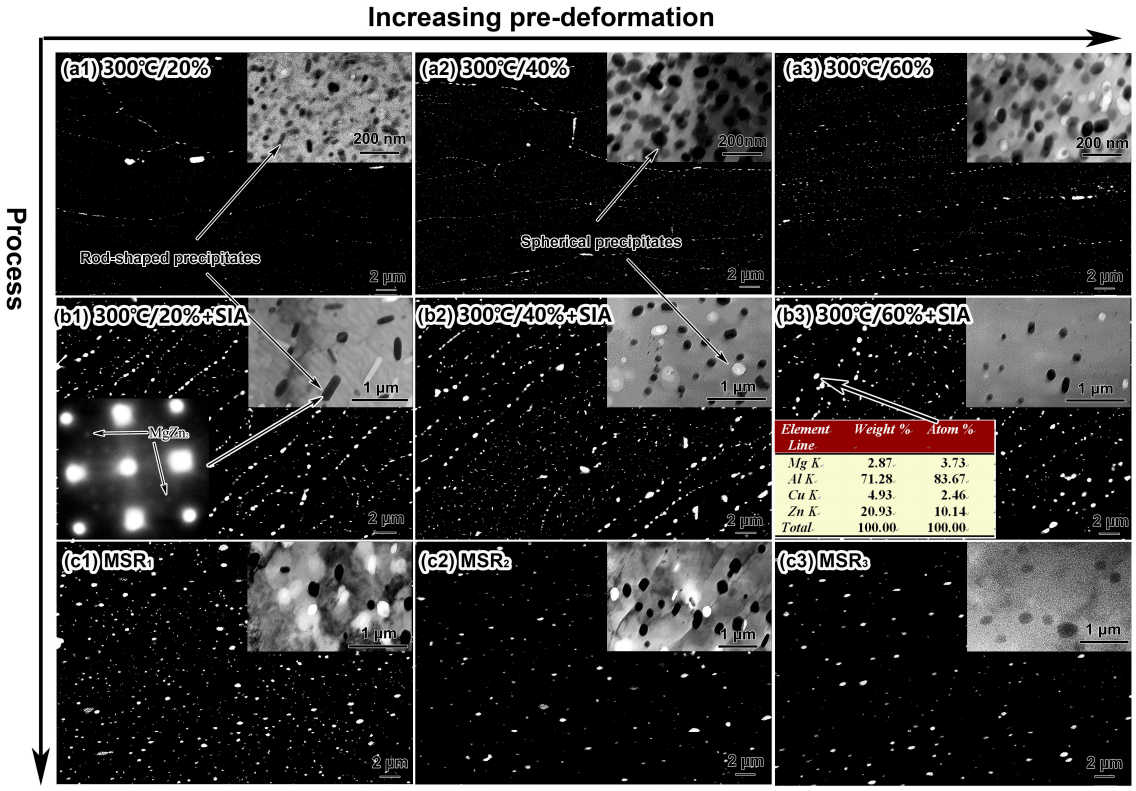

Figure 3. SEM images (by backscattered electron) with embedded TEM images of precipitates: (**a1**) 300 °C/20%; (**a2**) 300 °C/40%; (**a3**) 300 °C/60%; (**b1**) 300 °C/20% + SIA (with embedded SAED (selected area electron diffraction) patterns); (**b2**) 300 °C/40% + SIA; (**b3**) 300 °C/60% + SIA (with embedded EDS results); (**c1**) MSR_1; (**c2**) MSR_2; (**c3**) MSR_3.

In our previous work, it was proved that the second phase particles play a very important role [24,28,29] during TMPs. In this paper, the DIPs (deformation induced precipitates) obtained by pre-deformation also affected microstructure of the subsequent intermediate annealing. The pre-deformed samples then annealed at 430 °C for 5 min, morphology of precipitates changed as shown in Figure 3(b1–b3). Precipitates in (300 °C/20% + SIA) samples were rod-shaped or spherical, with the rod length of 200–500 nm, and a width of 50–150 nm (Figure 3(b1)). With increased pre-deformation, precipitates were gradually refined and spheroidized (Figure 3(b2,b3)). According to the embedded DIPs SAED, in Figure 3(b1), and EDS results, in Figure 3(b3), DIPs were proved to be $MgZn_2$ phase.

When new phases are precipitated from a parent phase, the change of Gibbs free energy during the whole process can be expressed as follows [30,31]:

$$\Delta G = V\Delta G_V + V\Delta G_\varepsilon + A\gamma \quad (1)$$

where V is the volume of new phase, ΔG_V is the free energy difference between new phase and parent phase per unit volume, ΔG_ε is the strain energy of new phase per unit volume, A is the total interfacial area of new phase, and γ is the interfacial energy between new phase and parent phase.

The area fraction of $MgZn_2$ phase in 7055 Al alloy remains unchanged under different deformations. Therefore, V, ΔG_V, and A are constant under different TMPs. The value of ΔG is determined by the relationship between γ and ΔG_ε. As shown in Figure 3(a1,b1), strain energy (ΔG_ε) is the main factor during deformation at 300 °C for 20%, so precipitates are rod-shaped. Defects induced by deformation also increase with deformation. When new phase particles precipitated at these defects, the defects were destroyed or disappeared, thus reducing the Gibbs free energy of the system [32].

When large deformation is introduced, the change of Gibbs free energy of the whole system can be expressed as [31,32]:

$$\Delta G' = V\Delta G_V + V\Delta G_\varepsilon + A\gamma + V\Delta G_B \quad (2)$$

where ΔG_B is the decrease of Gibbs free energy per unit volume (due to the introduction of abundant defects, the free energy will be reduced due to the precipitation at these defects).

The critical nucleation radius r^* of precipitates can be expressed as [32,33]:

$$r* = 2\gamma/(\Delta G_V + \Delta G_\varepsilon + \Delta G_B) \quad (3)$$

with the increased ΔG_B, (ΔG_V + ΔG_ε + ΔG_B) increases and r^* decreases, which leads to the increase of driving force $\Delta G'$ and the quantity of nucleation. Therefore, the surface energy (interfacial energy) plays a more important role than the strain energy. Moreover, the surface energy of spherical particles is the lowest, so the spheroidization of precipitates will be promoted after large deformation (Figure 3(a2,a3,b2,b3)).

Figure 3(c1–c3) shows SEM (TEM) images of the final-rolled 7055 Al alloy by different TMPs. With decreased deformation in the final hot rolling stage ($MSR_1 \rightarrow MSR_3$), the size of precipitates almost remains unchanged, but their density decreases. After statistics, it was found that the size of precipitates by different TMPs was similar (MSR_1: 110 nm; MSR_2: 140 nm; MSR_3: 150 nm) while their area fraction decreased from MSR_1 to MSR_3 (MSR_1: 6.2%; MSR_2: 5.1%; MSR_3: 4.4%). Compared with the final hot rolling temperature, pre-deformation temperature was relatively lower (300 < 400 °C), the atom movement was slow, and dislocation was inactive. Therefore, under the same deformation, the accumulated defects are more than those in the final hot rolling. These defects form fast diffusion channels, and accelerate the dissolution of precipitates during hot rolling. Thus, the larger the pre-deformation, the more defects can be accumulated, which leads to a faster re-dissolution rate of DIPs in the high temperature hot rolling stage.

The pinning force of precipitates on boundaries can be expressed as [34]:

$$P_Z = 3F_V\gamma_b/d \quad (4)$$

P_Z: Zener drag force, F_V: Volume fraction of precipitates, γ_b: Constant, d: Average diameter of precipitates.

The area fraction of precipitates decreases gradually from MSR_1 to MSR_3 (Figure 3(c1–c3)), but their sizes are similar, i.e., γ_b and d remain unchanged while F_V decreases. Therefore, during the hot rolling process, the pinning force of precipitates on boundaries gradually weakens.

Figure 4 shows the EBSD with embedded TEM images of (sub) grain structures. After deformation at 300 °C for 20%, dislocations were pinned by precipitates (Figure 4(a1), insert map). When deformation increased to 40%, more defects (such as dislocations) were introduced, dynamic recovery occurred, and dislocation cells were formed (Figure 4(a2)). With continued increasing of the deformation to 60%, dislocation cells grew up, but their boundaries were still pinned by precipitates, hard to form clear-cut subgrains (Figure 4(a3)). During the SIA process, the redissolution of precipitates, and recovery also affect substructures. The growth of precipitates follows the Ostwald ripening principle (smaller particles dissolve while larger grow up [35]). The remaining fine precipitates (incompletely dissolved) will continue to pin boundaries, while the fully dissolved or coarsened precipitates will lose their pinning effect. The (sub)grain boundaries and dislocations, without pinning hindrance become active, resulting in static recovery. Figure 4(b1–b3) embedded images show TEM images of substructure morphology of different samples after SIA treatment. At 300 °C/20% + SIA, samples underwent static recovery and dislocation rearrangement to form an ordered dislocation array. Banded structures (composed of dislocation array) were formed along the direction at about 45° to grain boundaries (Figure 4(b1)). With the increase of deformation, these banded structures gradually become equiaxed, and subgrains with clear boundaries were formed when deformation reached 60% (Figure 4(b2)).

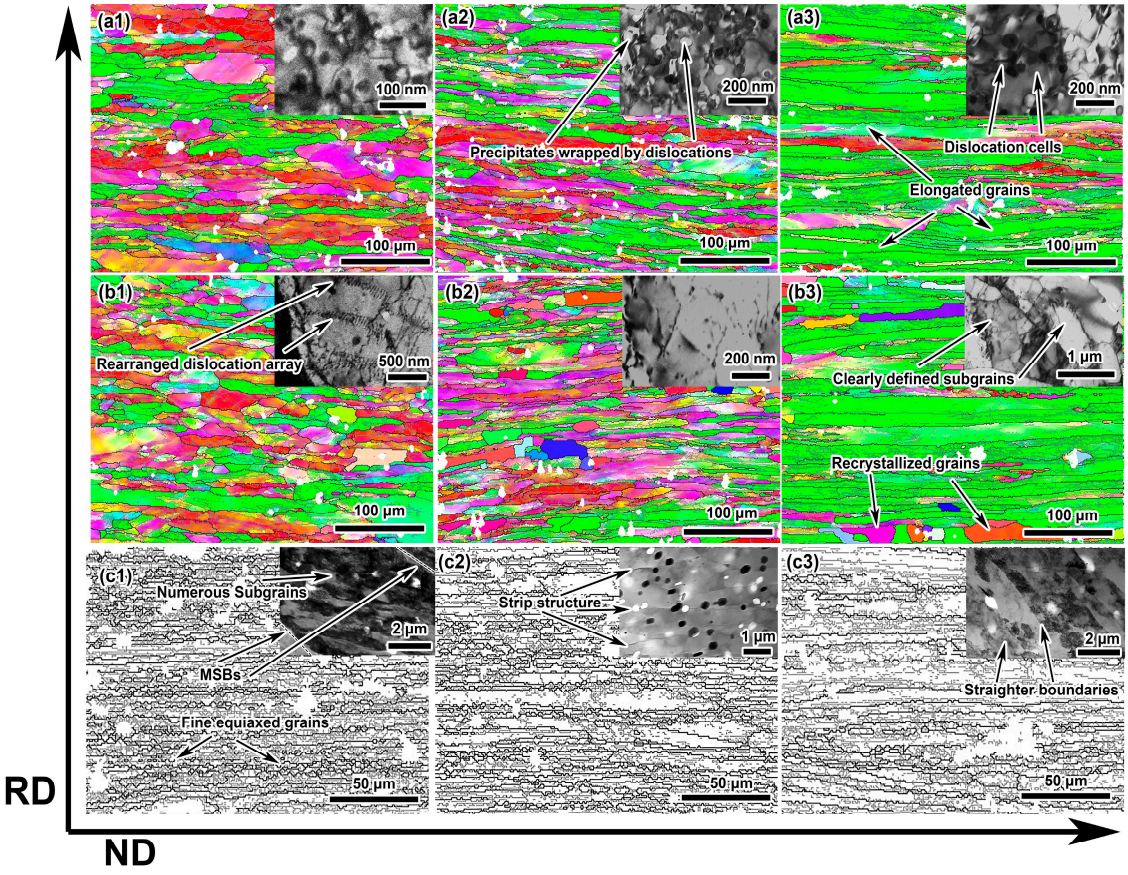

Figure 4. EBSD with embedded TEM images of (sub) grain structure: (**a1**) 300 °C/20%; (**a2**) 300 °C/40%; (**a3**) 300 °C/60%; (**b1**) 300 °C/20% + SIA; (**b2**) 300 °C/40% + SIA; (**b3**) 300 °C/60% + SIA; (**c1**) MSR_1; (**c2**) MSR_2; (**c3**) MSR_3.

SIA (annealing at 430 °C) can be considered as a high temperature recovery treatment (temperature >0.6 T_m, T_m: melting point of 7055 Al alloy, under which edge dislocations can obtain enough energy to climb), which can lead to the following results: Irregular dislocations were rearranged to form dislocation walls, for the reduction of elastic distortion energy (Figure 4(b1)); Partial dislocation walls (along the direction perpendicular to the slip plane, and with a certain orientation difference) were polygonal, and formed subgrains (Figure 4(b2,b3)). In the recovery stage, the driving force of polygonization came from the decrease of deformation storage energy, so the polygonal degree increases with deformation, and subgrains with clear boundaries were formed finally [32]. After SIA, fine precipitates (retained due to Ostwald role) could still pin boundaries, and a large quantity of sub-structures formed by static recovery at this stage, which underwent certain transformations in the final hot rolling, resulting in grain refinement (Figure 4(c1–c3)). Figure 4(c1) shows that in addition to forming a large quantity of subgrains, micro shear bands (MSBs) were observed after MSR_1 treatment, which are composed of a number of regularly arranged fine subgrains. According to Hurley P.J. [36] MSBs are transformed from deformation bands. MSBs can increase the fraction of LAGBs, refine subgrains, and become the preferred nucleation sites in the subsequent recrystallization treatment [36,37]. With decreased high-temperature deformation, clear banded structures were obtained by MSR_2 (40 + 40%), and precipitates were distributed along boundaries of the strip structure (Figure 4(c2)). When the high-temperature deformation reduced to 20% (MSR_3 60 + 20%), the banded structures were more obvious, and boundaries were straighter due to severe recovery (the reduction of pinning force) (Figure 4(c3)).

After pre-deformation, grains of all alloys were elongated (Figure 4(a1–a3)). A few equiaxed grains remained near the elongated grain boundaries. With the increased pre-deformation (20→60%), dynamic recovery was more serious, grain boundaries became straighter, grain widths became narrower, and the orientation was gradually closer to {101}.

After short-time high-temperature intermediate annealing at 430°C, obvious static recovery (the appearance of subgrains and increase of grain width) and static recrystallization (the formation of fine equiaxed grains) occurred (Figure 4(b1–b3)). Compared with SQ-7055, grain size was refined. However, due to lack of deformation storage energy, the complete recrystallization cannot take place, so strip-shaped grains were still dominant. With increased pre-deformation, dynamic recovery was more serious, with wider grain size.

After the final hot rolling (400 °C), obvious fibrous deformed ribbons were obtained. Fine equiaxed grains appeared near the original grain boundaries (Figure 4(c1–c3). The reason is that numerous substructures generated by SIA changed under the subsequent hot rolling (high temperature 400 °C and accumulated large deformation 80%). Activity of boundaries increased, and the LAGBs (subgrains) gradually stabilized and transformed into HAGBs (equiaxed grains) [37]. From MSR_1 to MSR_3, the increase of {101} oriented grains indicates that dynamic recovery (recrystallization) was gradually weakened (Figure 4(c1–c3)). The higher the deformation temperature is, the higher the activity of dislocations and (sub)grain boundaries will be, and it is easier for their migration and merging. Moreover, MSR_1 (300 °C, 20% + 400 °C, 60%) mainly deformed at high temperature compared with MSR_3 (300 °C, 60% + 400 °C, 20%) leading to more severe dynamic recovery, and more obvious grain refinement.

Figure 5 shows the XRD spectrum and precipitation statistics of 7055 Al alloy treated by different processes. It can be seen that the second phase particles after pre-deformation are mainly $MgZn_2$, which is consistent with the SAED in Figure 3(b1) and EDS results in Figure 3(b3) (Figure 5a). After different pre-deformations at 300 °C, the intensity of $MgZn_2$ peak remained almost the same, which reflects the similar precipitate content (i.e., area fraction) [38]. This is consistent with the statistical trend in Figure 5d. Figure 5b shows the XRD spectrum of 7055 Al alloy after SIA. As the intermediate annealing temperature (430 °C) is close to the solution temperature (475 °C), compared with the peak of pre-deformation (Figure 5a), the diffraction peak intensity of SIA is weakened, indicating that precipitates were re-dissolved during SIA. However, the annealing time is short (5 min), so the

redissolution maybe insufficient. Moreover, the intensity of $MgZn_2$ diffraction peaks in Figure 5b decrease with the increased pre-deformation (20→60%) in the SIA stage, which may be related to the increased defects accelerating precipitate re-dissolution. Furthermore, from the XRD spectrum of the finally rolled alloy (Figure 5c), with the reduced final rolling deformation (from MSR_1 to MSR_3 60→20%), the intensity of $MgZn_2$ peak gradually decreases, indicating the decreased $MgZn_2$ content. Similarly, this is consistent with the statistical trend in Figure 5d. Low pre-deformation temperature and weak dynamic recovery can lead to more introduction of defects, and accelerate the redissolution of precipitates, so the content of $MgZn_2$ decreases with the decreased final rolling deformation.

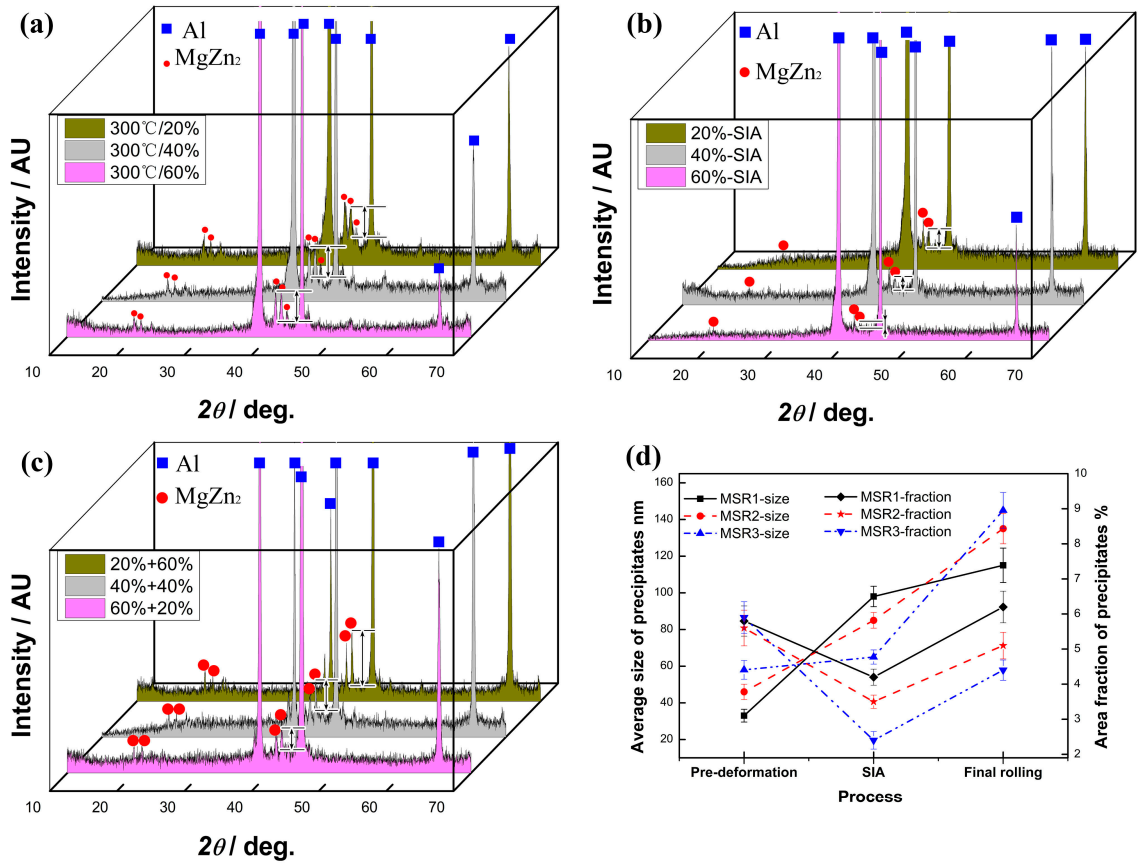

Figure 5. XRD patterns of alloys: (**a**) after pre-deformation, (**b**) after SIA, and (**c**) after the final hot rolling; (**d**) statistics of average size and area fraction of precipitates.

3.3. Analysis of Grain Refinement

To sum up, grain refinement is mainly achieved by dislocation cancellation and rearrangement, which transforms LAGBs into HAGBs. Precipitates play an important role during the whole process. Many models have been used to describe the effects of particles/precipitates and substructures on grain refinement [39,40]. According to these models and the analysis results in Section 3.2, the specific process of grain refinement in MSR can be summarized as follows: (1) Plenty of spherical precipitates wrapped by dislocations were produced during pre-deformation at 300°C. After further recovery, dislocation cells were formed, seen in Figure 4(a1–a3) and Figure 6b; (2) During SIA treatment, the activity of dislocations increased, while precipitates partially dissolved, resulting in weakening of the pinning effect. Dislocations become ordered and rearranged to form subgrains, as shown in Figure 4(b1–b3) and Figure 6c; (3) In the high temperature final rolling stage, the accumulated strain increased, and the grains further elongated (Figure 4(c1–c3)). Due to the pinning of precipitates and the accumulation of strain (absorption of defects such as dislocations), sub-grain boundaries gradually stabilized, and LAGBs transformed into HAGBs, with a reduced proportion of LAGBs (Figure 6e,f). Fine equiaxed

grains appeared near original grain boundaries, so as to realize grain refinement (Figure 4(c1–c3) and Figure 6e,f).

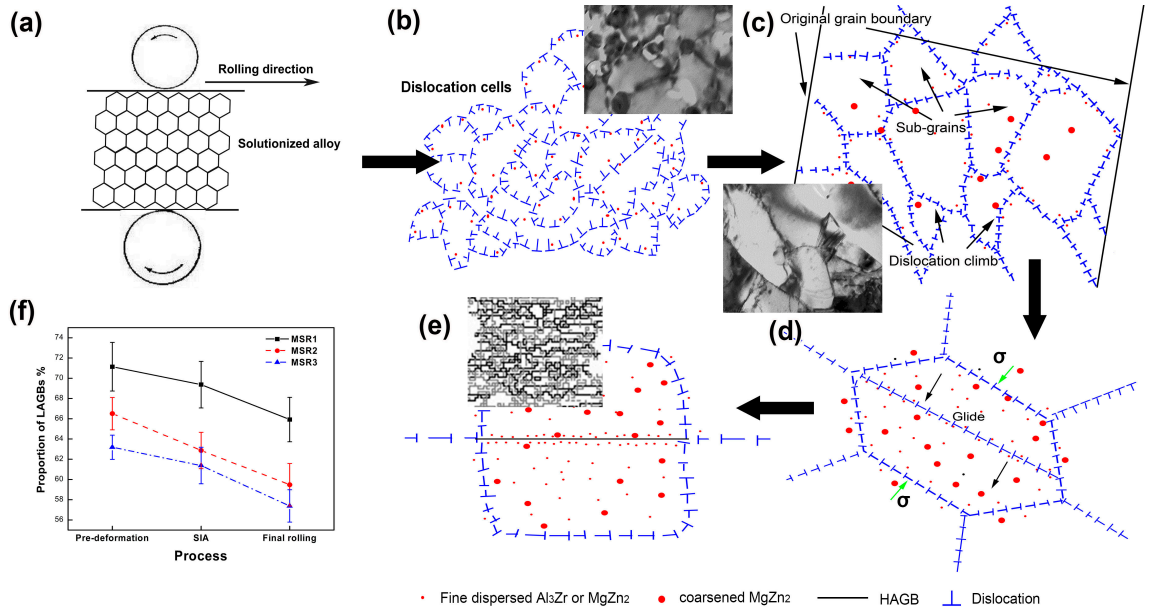

Figure 6. Schematic diagram of grain refinement: (**a**) deformation induced by rolling; (**b**) after pre-deformation; (**c**) after SIA; (**d**) with further hot deformation; (**e**) after final hot rolling; (**f**) statistical diagram of LAGBs.

3.4. Microstructure and Mechanical Properties of the Rolled Sheets after Solution and Aging Treatment

Figure 7 shows OM and EBSD maps of 7055 Al alloy (processed by CHR and MSR) after solution treatment at 475 °C for 0.5 h. Typical recrystallization structures were formed by both processes, but the former (CHR) was extremely uneven (Figure 7(d1,d2)), with more elongated banded structures and less equiaxed grains (diameter about 35 μm). However, MSR plates show different degrees of grain refinement, the specific grain size is shown in Figure 8c. Grain refinement of MSR_1 was the most obvious with plenty of fine equiaxed grains and uniform grain size. Less strip structures with more equiaxed grains appeared in MSR_1. Some LAGBs appear in the grain interior. From MSR_1 to MSR_3, the length of the recrystallized grains increased, while the width decreased with the decreased final rolled deformation (80→20%), while the quantity of fine equiaxed grains decreased (Figure 7(a1–c1) and Figure 8c), which means the effect of grain refinement was weakened.

Room temperature tensile engineering stress-strain curves, and the ultimate tensile strength (UTS), yield strength (YS), and elongation (δ), of all rolled plates after solution and T6 aging are shown in Figure 8a,b. The tensile strength and elongation of CHR alloy are 605 MPa and 14%, respectively, while that of MSR_1 alloy are 604 MPa and 18.2% (specimens break after a certain necking stage). Due to the same solution aging process, the difference of mechanical properties is mainly related to the difference of microstructure caused by TMPs. It has been proved that grain refinement plays a limited role in improving strength of precipitation strengthening alloys, like 7xxx series Al alloy [17,22,29]. In another way, grain refinement can increase the quantity of grains per unit volume, reduce the nucleation of crack, and increase the resistance to crack propagation [25]. The coordination between grains during plastic deformation in equiaxed fine-grained samples is better than that in coarse-grained samples, leading to more uniform deformation, so as to increase the resistance of crack initiation, improve the dislocation storage capacity and elongation of the alloy. Therefore, the plasticity of fine-grained alloy is much higher than that of coarse-grained alloy.

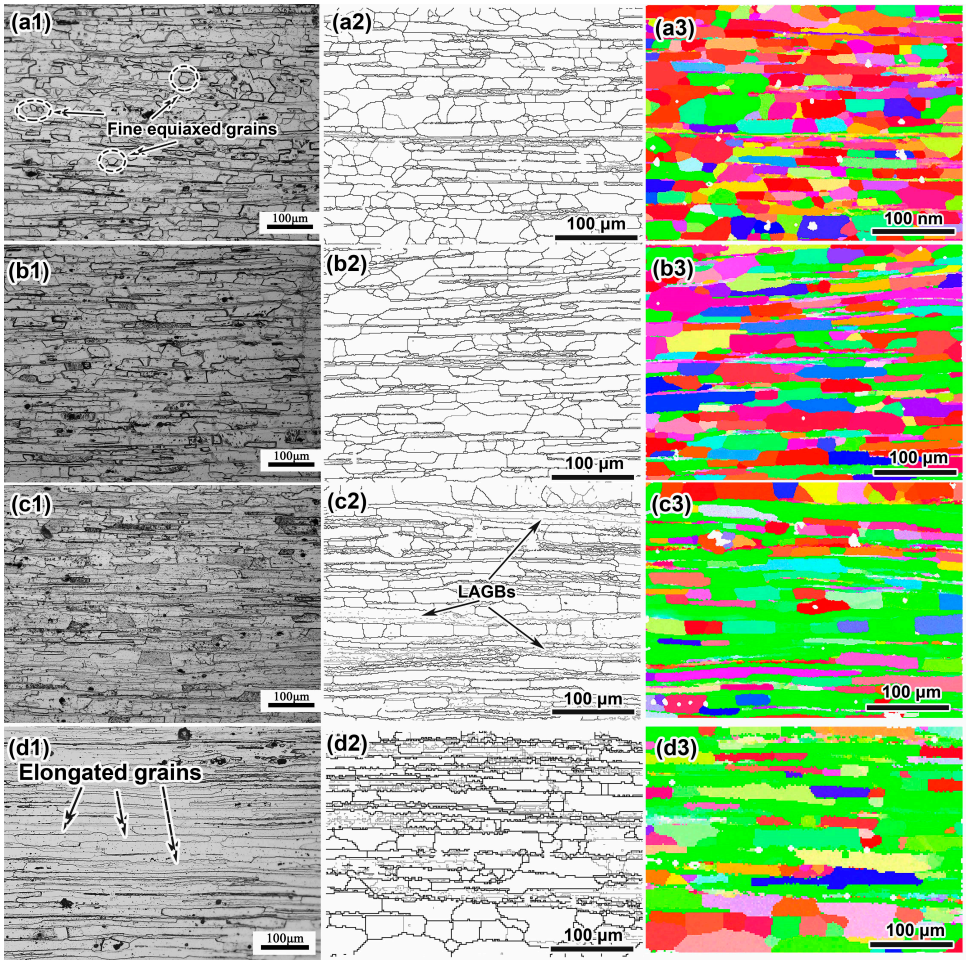

Figure 7. OM (**a1–d1**) and EBSD maps (**a2–d2** for grain boundaries, **a3–d3** for grain orientations) of alloys after recrystallization: (**a**) MSR_1; (**b**) MSR_2; (**c**) MSR_3; (**d**) CHR.

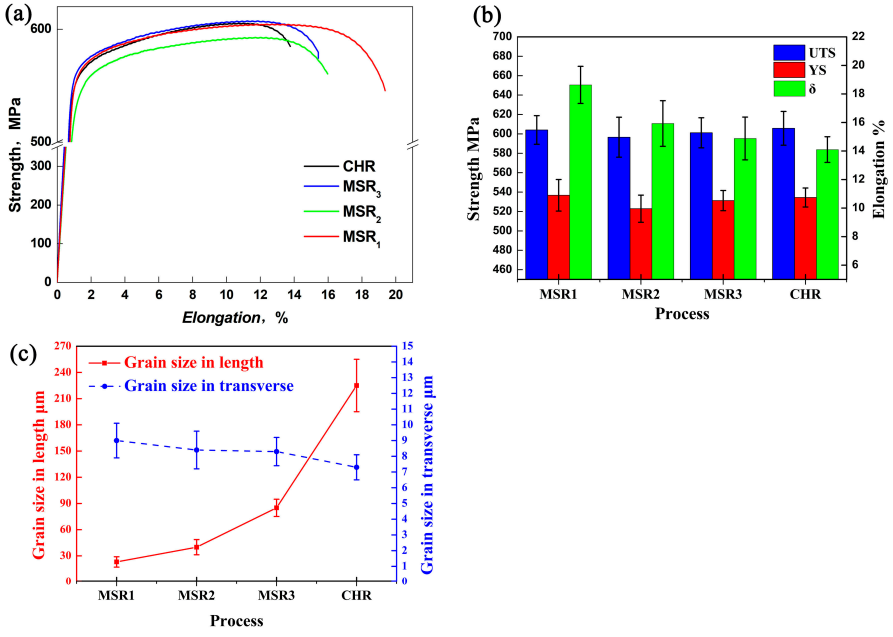

Figure 8. (**a**) Engineering stress–strain curves; (**b**) the UTS (Ultimate tensile strength), YS (yield strength) and δ (elongation) of all processed alloys after T6 aging; (**c**) the average grain size after recrystallization.

Figure 9 shows the fracture surface of the MSR_1 sample (with the highest elongation) and CHR sample (with the lowest elongation), respectively. The fracture morphology is closely related to the fracture mode and plasticity. As shown in Figure 9(b1,b2), the fracture surface of the CHR sample is relatively smooth with an obvious "fluvial step" structure. A small amount of coarse dimples also appear on the CHR fracture surface, with crushed coarse particles inside them, which indicates that CHR alloy is mainly brittle transgranular fracture mode. However, in the MSR_1 alloy (Figure 9(a1,a2)), a large quantity of fine dimples and tearing edges can be seen, with a quite uneven fracture surface. This means the crack propagation direction changes many times during the tensile fracture process. The fracture mode of MSR_1 is a mixture of transgranular fracture (a great deal of fine deep dimples) and intergranular fracture (plenty of tearing edges). Between them, transgranular fracture is dominant, which indicates that MSR_1 alloy is ductile fracture. Therefore, the plasticity (elongation) of MSR_1 alloy is much higher than that of CHR.

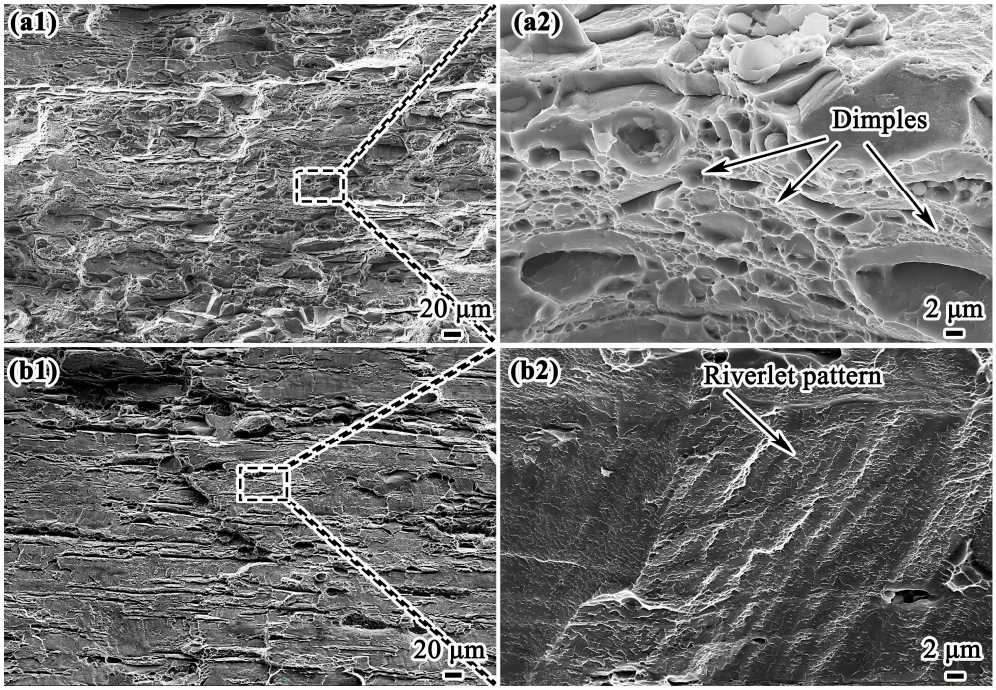

Figure 9. Fracture surfaces of the failed T6 specimens: (**a1**,**a2**) MSR_1; (**b1**,**b2**) CHR.

4. Conclusions

In this paper, a new thermomechanical process (pre-deformation + short period intermediate annealing + final hot rolling) based on deformation induced precipitates was investigated, as well as the effect of parameters on precipitates. The main conclusions can be summarized as follows:

(1) With increased pre-deformation, precipitates were spheroidized gradually with increased size and decreased density, but the area fraction remained almost the same. However, further increased pre-deformation (60→80%) will increase the size of precipitates and weaken the pinning effect on dislocations, which is not conducive to grain refinement in subsequent processes.

(2) Dislocations induced by pre-deformation were entangled and recovered to form dislocation cells. The spheroidized $MgZn_2$ particles pinned dislocations and boundaries, which led to the formation of numerous subgrains during the short period intermediate annealing. The transformation of low angle grain boundaries into high angle grain boundaries could have been accelerated by the pinning effect of precipitates and accumulated deformation during further hot rolling. The optimum TMP for grain refinement was obtained: solid solution + pre-deformation (300 °C/20%) + intermediate annealing (430 °C/5 min) + hot deformation (400 °C/60%).

(3) The plasticity of alloys can be obviously improved by grain refinement. In particular, the elongation of the MSR_1 samples in T6 state could be increased by 25% compared with those of the CHR sample. Grain refinement plays a key role.

Author Contributions: Conceptualization, J.Z. (Jinrong Zuo), L.H. and J.Z. (Jishan Zhang); methodology, J.Z. (Jinrong Zuo) and W.P.; formal analysis, J.Z. (Jinrong Zuo); investigation, J.Z. (Jinrong Zuo), X.S. and A.Y.; writing—original draft preparation, J.Z. (Jinrong Zuo); writing—review and editing, L.H., X.S., W.P., A.Y. and J.Z. (Jishan Zhang); visualization, J.Z. (Jinrong Zuo), X.S., W.P. and A.Y.; supervision, X.S. and J.Z. (Jishan Zhang); project administration, X.S. and J.Z. (Jishan Zhang). All authors have read and agreed to the published version of the manuscript.

Funding: This research is supported by the Natural Science Foundation of Zhejiang (No. LQ19E010003), the Major State Research and Development Program of China (No. 2016YFB0300801), the State Key Laboratory for Advanced Metals and Materials of China (No. 2019-Z16), and Sponsored by the K.C. Wong Magna Fund in Ningbo University.

Conflicts of Interest: The authors declare no conflict of interest.

References

1. Vincze, G.; Simões, F.J.; Butuc, M.C. Asymmetrical rolling of aluminum alloys and steels: A review. *Metals* **2020**, *10*, 1126. [CrossRef]
2. Rambabu, P.; Prasad, N.E.; Kutumbarao, V.V.; Wanhill, R.J.H. *Aluminium Alloys for Aerospace Applications*; Springer: Singapore, 2017.
3. Ghosh, A.; Ghosh, M.; Gudimetla, K.; Kalsar, R.; Kestens, L.A.I.; Kondaveeti, C.S.; Ravisankar, B. Development of ultrafine grained Al–Zn–Mg–Cu alloy by equal channel angular pressing: Microstructure, texture and mechanical properties. *Arch. Civ. Mech. Eng.* **2020**, *20*, 1–17. [CrossRef]
4. Shafei, M.A.; Hosseinipour, S.J.; Rajabi, M. Microstructural characterization of nanostructured Al-Zn-Mg-Cu alloy during mechanical alloying and subsequent annealing. *Adv. Mat. Res.* **2013**, *829*, 57–61. [CrossRef]
5. Li, H.; Cao, F.; Guo, S.; Jia, Y.; Zhang, D.; Liu, Z. Effects of Mg and Cu on microstructures and properties of spray-deposited Al-Zn-Mg-Cu alloys. *J. Alloy. Compd.* **2017**, *719*, 89–96. [CrossRef]
6. Zhang, H.; Li, L.; Yuan, D.; Peng, D. Hot deformation behavior of the new Al-Mg-Si-Cu aluminum alloy during compression at elevated temperatures. *Mater. Charact.* **2007**, *58*, 168. [CrossRef]
7. Tang, J.; Zhang, H.; Teng, J.; Fu, D.; Jiang, F. Effect of Zn content on the static softening behavior and kinetics of Al–Zn–Mg–Cu alloys during double-stage hot deformation. *J. Alloy. Compd.* **2019**, *806*, 1081–1096. [CrossRef]
8. Yu, H.; Xin, Y.; Wang, M.; Liu, Q. Hall-Petch relationship in Mg alloys: A review. *J. Mater. Sci. Technol.* **2017**, *34*, 248–256. [CrossRef]
9. Huang, T.; Shuai, L.; Wakeel, A.; Wu, G.; Hansen, N.; Huang, X. Strengthening mechanisms and hall-Petch stress of ultrafine grained Al-0.3%Cu. *Acta Mater.* **2018**, *156*, 369–378. [CrossRef]
10. Lotkov, A.; Baturin, A.; Kopylov, V.; Grishkov, V.; Laptev, R. Structural defects in TiNi-based alloys after warm ECAP. *Metals* **2020**, *10*, 1154. [CrossRef]
11. Xing, J.; Soda, H.; Yang, X.; Miura, H.; Sakai, T. Ultra-fine grain development in an AZ31 magnesium alloy during multi-directional forging under decreasing temperature conditions. *Mater. Trans.* **2005**, *46*, 1646–1650. [CrossRef]
12. Shi, J.T.; Hou, L.G.; Zuo, J.R.; Zhuang, L.Z.; Zhang, J.S. Cryogenic rolling-enhanced mechanical properties and microstructural evolution of 5052 Al-Mg alloy. *Mat. Sci. Eng. A* **2017**, *701*, 274–284. [CrossRef]
13. Wang, X.F.; Guo, M.X.; Chen, Y.; Zhu, J.; Zhang, J.S.; Zhuang, L.Z. Effect of thermomechanical processing on microstructure, texture evolution, and mechanical properties of Al-Mg-Si-Cu alloys with different zn contents. *Metall. Mater. Trans. A* **2017**, *48*, 3540–3558. [CrossRef]
14. Yi, S.; Victoria-Hernandez, J.; Kim, Y.M.; Letzig, D.; You, B.S. Microstructure and property relationship controllable by thermomechanical processing of Mg-Al-Zn-Y-Ca alloy sheets. *Acta Phys. Pol. A* **2018**, *134*, 838–841. [CrossRef]
15. Yan, L.M.; Shen, J.; Li, Z.B.; Li, J.P. Effect of deformation temperature on microstructure and mechanical properties of 7055 aluminum alloy after heat treatment. *Trans. Nonferrous Met. Soc. China* **2013**, *23*, 625–630. [CrossRef]

16. Russo, E.D.; Conserva, M.; Buratti, M.; Gatto, F. A new thermo-mechanical procedure for improving the ductility and toughness of AlZnMgCu alloys in the transverse directions. *Mat. Sci. Eng.* **1974**, *14*, 23–36. [CrossRef]
17. Waldman, J.; Sulinski, H.; Markus, H. The effect of ingot processing treatments on the grain size and properties of Al alloy 7075. *Metall. Mater. Trans. B* **1974**, *5*, 573. [CrossRef]
18. Wert, J.A.; Paton, N.E.; Hamilton, C.H.; Mahoney, M.W. Grain refinement in 7075 aluminum by thermomechanical processing. *Metall. Mater. Trans. A* **1981**, *12*, 1267. [CrossRef]
19. Esmaeili, S.; Lloyd, D.J.; Jin, H. A thermomechanical process for grain refinement in precipitation hardening AA6xxx aluminum alloys. *Mater. Lett.* **2011**, *65*, 1028–1030. [CrossRef]
20. Robson, J.D. Microstructural evolution in aluminium alloy 7050 during processing. *Mat. Sci. Eng. A* **2004**, *382*, 112–121. [CrossRef]
21. Li, X.M.; Starink, M.J. Effect of compositional variations on characteristics of coarse intermetallic particles in overaged 7000 series aluminium alloy. *Mater. Sci. Technol.* **2001**, *17*, 1324–1328.
22. Knipling, K.E.; Dunand, D.C.; Seidman, D.N. Criteria for developing castable, creep-resistant aluminum-based alloys—A review. *Z. Met.* **2006**, *97*, 246–265. [CrossRef]
23. Zuo, J.R.; Hou, L.G.; Shu, X.D.; Peng, W.F.; Yin, A.M.; Zhang, J.S. Grain refinement assisted by deformation enhanced precipitates through thermomechanical treatment of AA7055 al alloy. *Metals* **2020**, *10*, 594. [CrossRef]
24. Zuo, J.R.; Hou, L.G.; Shi, J.T.; Cui, H.; Zhuang, L.Z.; Zhang, J.S. Effect of deformation induced precipitation on grain refinement and improvement of mechanical properties AA 7055 aluminum alloy. *Mater. Charct.* **2017**, *130*, 123–134. [CrossRef]
25. Yu, D. Effect of interstage homogenizing treatment on homogenization degree and overburnt temperature of 7AO4 alloy. *Alum. Fabr.* **2003**, *3*, 23–26.
26. Freiberg, D.; Zhu, W.; Park, J.S.; Almer, J.D.; Sanders, P. Precipitate characterization in model Al-Zn-Mg-(Cu) alloys using small-angle X-ray scattering. *Metals* **2020**, *10*, 959. [CrossRef]
27. Zuo, J.R.; Hou, L.G.; Shi, J.T.; Cui, H.; Zhuang, L.Z.; Zhang, J.S. Effect of deformation induced precipitation on dynamic aging process and improvement of mechanical/corrosion properties AA7055 aluminum alloy. *J. Alloy. Compd.* **2017**, *708*, 1131–1140. [CrossRef]
28. Zuo, J.R.; Hou, L.G.; Shi, J.T.; Cui, H.; Zhuang, L.Z.; Zhang, J.S. Enhanced plasticity and corrosion resistance of high strength Al-Zn-Mg-Cu alloy processed by an improved thermomechanical processing. *J. Alloy. Compd.* **2017**, *716*, 220–230. [CrossRef]
29. Zuo, J.R.; Hou, L.G.; Shi, J.T.; Cui, H.; Zhuang, L.Z.; Zhang, J.S. The mechanism of grain refinement and plasticity enhancement by an improved thermomechanical treatment of 7055 Al alloy. *Mat. Sci. Eng. A* **2017**, *702*, 42–52. [CrossRef]
30. Liddicoat, P.V.; Liao, X.-Z.; Zhao, Y.; Zhu, Y.; Murashkin, M.Y.; Lavernia, E.J. Nanostructural hierarchy increases the strength of aluminium alloys. *Nat. Commun.* **2010**, *1*, 63. [CrossRef]
31. Doherty, R.D. Physical metallurgy. In *Physical Metallurgy*; Cahn, R.W., Haasen, P., Eds.; North-Holland: Oxford, UK, 1996; pp. 1363–1505.
32. Yu, Y.N. *Principles of Metallurgy*; Metallurgical Industry Press: Beijing, China, 2000; pp. 481–490.
33. Yujing, L. Grain Refinement of 7050 Aluminum Alloy and Its Mechanical Behavior by Hot Deformation Based on Strain-Induced Precipitation. Ph.D. Thesis, University of Science and Technology, Beijing, China, 2012.
34. Zener, C. Theory of growth of spherical precipitates from solid solution. *Appl. Phys. Lett.* **1949**, *20*, 950. [CrossRef]
35. Chalendar, J.A.; de Garing, C.; Benson, S.M. Pore-scale modelling of Ostwald ripening. *J. Fluid. Mech.* **2018**, *835*, 363–392. [CrossRef]
36. Hurley, P.J.; Humphreys, F.J. The application of EBSD to the study of substructural development in a cold rolled single-phase aluminium alloy. *Acta Mater.* **2003**, *51*, 1087. [CrossRef]
37. Sakai, T.; Miura, H.; Goloborodko, A.; Sitdikov, O. Ultrafine grain formation in ferritic stainless steel during severe plastic deformation. *Acta Mater.* **2009**, *57*, 153. [CrossRef]
38. Lang, Y.J.; Cui, H.; Cai, Y.H.; Zhang, J.S. Effect of strain-modified particles on the formation of fined grains and the properties of AA7050 alloy. *Mater. Design* **2012**, *39*, 220. [CrossRef]

39. Lang, Y.J.; Zhou, G.; Hou, L.G.; Zhang, J.S.; Zhuang, L.Z. Significantly enhanced the ductility of the fine-grained Al–Zn–Mg–Cu alloy by strain-induced precipitation. *Mater. Des.* **2015**, *88*, 625–631. [CrossRef]
40. Huo, W.T.; Hou, L.G.; Zhang, Y.; Zhang, J.S. Warm formability and post-forming microstructure/property of high-strength AA 7075-T6 Al alloy. *Mat. Sci. Eng. A* **2016**, *675*, 44–54. [CrossRef]